Isothermal Reduction of Oxide Scale on Hot-Rolled, Low-Carbon Steel in 10 pct H_2-Ar

YONGQUAN HE, TAO JIA, ZHIFENG LI, GUANGMING CAO, ZHENYU LIU, and JUN LI

The isothermal reduction of oxide scale on hot-rolled, low-carbon steel strip in 10 pct H_2-Ar mixtures in the temperature range of 673 K to 1073 K (400 °C to 800 °C) was investigated by using a thermo-gravimetric analyzer (TGA). During heating under an argon atmosphere, magnetite/iron eutectoid and proeutectoid magnetite in the oxide scale successively transformed into wüstite at a temperature above 843 K (570 °C). The kinetic plot of the isothermal reduction assumes a sigmoid shape, including induction, acceleration, and finally the decaying stage. Fitting the kinetic curve to mathematical models, the reaction at 1073 K (800 °C) and 773 K (500 °C) were determined to be controlled by phase-boundary-controlled reaction and three-dimensional growth of nuclei, respectively. The reduction product varies with temperature and itself affects the kinetics. Porous and dense iron were, respectively, obtained below and above 873 K (600 °C). A ''rate-minimum'' was observed at 973 K (700 °C) due to the formation of dense iron that blocks the gas diffusion. Due to the structural transformation of oxide scale during heating, the reactant depends on the heating process. However, compared with the oxide scale structure, the temperature is more important in determining the reduction kinetics at temperatures above 973 K (700 °C).

DOI: 10.1007/s11661-016-3647-8
© The Minerals, Metals & Materials Society and ASM International 2016

I. INTRODUCTION

HOT-ROLLED steel strips are covered with oxide scale film, which is commonly descaled by chemical agents such as HCl, H_2SO_4. Acid pickling provides perfectly cleaned surface, which creates serious environmental pollutions and corrosion of production facilities. Alternatively, mechanical descaling technology such as dry shot blasting was developed, but it needs a large-size blasting chamber and dust collection systems that make it impractical for coils of hot-rolled steel. Another promising descaling method is Eco Pickled Surface (EPS), which uses a mixture of liquid carrier and abrasive material to impinge against the moving strip of steel to achieve a complete scale removal. The EPS-processed steel was found to be equivalent or superior to conventional acid-pickled steel.[1] In recent years, ''acid-free descaling'' technology, where hydrogen was employed as the agent for the reduction of oxide scale, emerges as another competitive descaling method due to its cleanness and environmental-friendly characteristics.

The oxide scale film on the hot-rolled, low-carbon steel usually consists of wüstite, magnetite, and hematite. The reduction of iron oxides in bulk has been one of the most frequently studied physical metallurgy topics.[2–5] For the reduction kinetics of iron oxides, there are two types of fractional reduction: (α) *vs* time (t) plots depending on the reduction condition (*e.g.*, temperature, reduction agent). The first one is sigmoid shaped, including an induction period, an acceleratory period, and finally a decaying period. This type of plot is usually found with reduction processes at low and moderate temperatures. For the second type of α–t plot, the induction period is negligible.[6] Except the kinetics, the morphology of reduction products also varies with the reduction condition and can be primarily classified into three types: dense iron; porous iron,[3,7–10] which was specially characterized by the diameters and spacing of gas pores; and whisker.[11–13]

The gas reduction of iron oxide scale, like every gas–solid reaction, includes gas–gas diffusion, gas–solid diffusion, and chemical reaction.[15] Efforts have been made to study the internal mechanism for reduction of iron oxides. Using hydrogen, Moukassi[14] studied the isothermal reduction kinetics of pure wüstite single crystal and found a ''rate minimum'' at 973 K (700 °C). Detailed analysis indicated that it was associated with the dense iron layer, which blocked the diffusion path of hydrogen. The grain boundary also plays an important role during the gaseous mass diffusion. Bahgat *et al.*[16–18] studied the effect of grain boundaries on

YONGQUAN HE, Ph.D. Student, formerly with the State Key Laboratory of Rolling and Automation, Northeastern University, Shenyang 110819, P.R. China, is now Lecturer with the School of Mechatronics Engineering, Zhengzhou University of Aeronautics, Zhengzhou 450015, P.R. China. Contact e-mail: hyquan3000@gamil.com.cn TAO JIA and GUANGMING CAO, Associate Professors, ZHIFENG LI, Ph.D. Student, and ZHENYU LIU, Professor, are with the State Key Laboratory of Rolling and Automation, Northeastern University. Contact e-mail: zyliu@mail.neu.edu.cn JUN LI, Lead Researcher, is with the Central Research Institute of Baosteel Group, Shanghai 201900, P.R. China.

Manuscript submitted April 7, 2015.
Article published online August 4, 2016

the surface rearrangement and iron nucleation during the isothermal reduction of wüstite. Due to the fast transportation of electron hole and Fe^{2+} ions near the grain boundary, the surface rearrangement dominantly occurs away from grain boundaries and then the iron is nucleated near grain boundaries.

For industrial applications, the reduction of oxide scale by hydrogen, as an alternative to conventional continuous strip pickling, has been investigated by several researchers.[19–21] Shi *et al.*[22] studied the reduction of oxide scale using pure carbon monoxide (CO). The oxide scale transformed into single wüstite during the heating to 1003 K (730 °C), and the majority of wüstite has been reduced into porous iron after reduction at 1003 K (730 °C) for 3 minutes. Guan *et al.*[23] investigated the isothermal reduction of hot-rolled strip scale by 20 pct hydrogen using TGA and concluded that the reduction process is controlled by growth of nuclei in the temperature range of 643 K to 823 K (370 °C to 550 °C).

In general, except the reduction condition, the important factors that affect the isothermal reduction kinetics include the morphology[24,25] (type of iron oxide, thickness, and distribution) and defect (porosity and crack) of the hot-rolled strip scale, as well as the phase transition during the heating to the isothermal reaction temperature. The purpose of this work is to study the isothermal reduction behavior of the oxide scale in a mixed gas containing low concentration of hydrogen. Based on the modeling methodology and microstructure examination, the reduction mechanism that varies with temperature is revealed. The effect of oxide scale structure on reduction kinetics is also preliminarily addressed.

II. EXPERIMENTAL PROCEDURE

A. *Materials and Methods*

TGA samples were prepared from a commercial hot-rolled, low-carbon steel strip with the chemical composition of 0.045C-0.025Si-0.2Mn-0.015P-0.007S-0.024Al (in mass pct). The sample size was 2.3 mm × 8 mm × 10 mm. Prior to each test, samples were cleaned by an ultrasonic cleaner. The initial sample weight in all cases was 1206 ± 5 mg.

B. *Thermal Simulation*

The transformation behavior of the oxide scale during heating under argon atmosphere was investigated by using a MMS-300 thermomechanical simulator. The sample was heated at a rate of 40 K/min and then quenched at different temperatures to exam the high-temperature microstructure.

C. *Isothermal Reduction*

The isothermal reduction was performed using TGA (Setsys Evolution 1750, SETARAM) with a sensibility of 30 μg. As shown in Figure 1(a), the sample was heated at a rate of 40 K/min in an argon flow. After reaching the desired isothermal reduction temperature, argon was immediately replaced by a dried mixture of 10 pct H_2-90 pct Ar with water vapor content lower than 0.06 pct. According to the gas flow rate of 200 mL/min, the average velocity was calculated to be 3.5 cm/s. A thermocouple was placed away from the sample at a distance of 2 mm. Variation of the sample weight and temperature as a function of time were recorded by a data acquisition system. After the isothermal reduction of 30 minutes, the gas mixture was switched back to argon and the sample was cooled at a rate of 99 K/min to room temperature. Finally, a repeated process was performed to record a background curve. Using the Calisto software, the stored heating data were then subtracted to avoid the effect of the air turbulence.

D. *Effect of Structure on the Reduction*

The effect of the structure on the reduction of oxide scale was investigated using TGA. The sample was heated to 1073 K (800 °C). After 2 minutes of annealing, the sample was rapidly cooled to 973 K (700 °C) to maintain the high-temperature structure. Reduction by the gas mixture of 10 pct H_2-Ar was then performed. To determine the decisive factors in reduction, the sample was reduced at 973 K (700 °C) for 10 minutes first, then elevated to 1073 K (800 °C), and continually reduced for 20 minutes. These two experiments described earlier are schematically illustrated in Figure 1(b) and (c).

After thermal cycle, samples were mounted in Bakelite, the sample cross sections were successively ground using SiC-papers with 800, 1000, and 1200 grit and polished with 2.5-μm diamond paste. To enhance the electrical conductivity around the oxide scale, the metallographic specimen was coated with carbon using a high vacuum carbon coater (Cressington 208C). The oxide scales, as well as the reduction products, were examined by electron probe microanalysis (JXA-8530F, JEOL).

III. RESULTS AND DISCUSSION

A. *Phase Transformation during Heating*

Figure 2(a) shows a typical oxide scale structure on a hot-rolled steel strip, which includes magnetite and "lamellar magnetite + iron" eutectoid. The upper dark side and lower bright side of the images is the resin and steel substrate, respectively. The oxide scale layer runs horizontally through the middle of the image. When the sample was quenched at 868 K (595 °C) during heating at a rate of 40 K/min, eutectoid has partially transformed into wüstite (Figure 2(b)). At 973 K (700 °C), this inverse eutectoid transformation was almost completed, whereas the transformation of proeutectoid magnetite to wüstite is still in progress (see the outer thick layer of magnetite in Figure 2(c)). The complete transformation of eutectoid and pro-eutectoid magnetite into wüstite was achieved at 1023 K (750 °C) (Figure 2(d)), and the oxide scale then developed a bilayer structure with outermost magnetite and interior

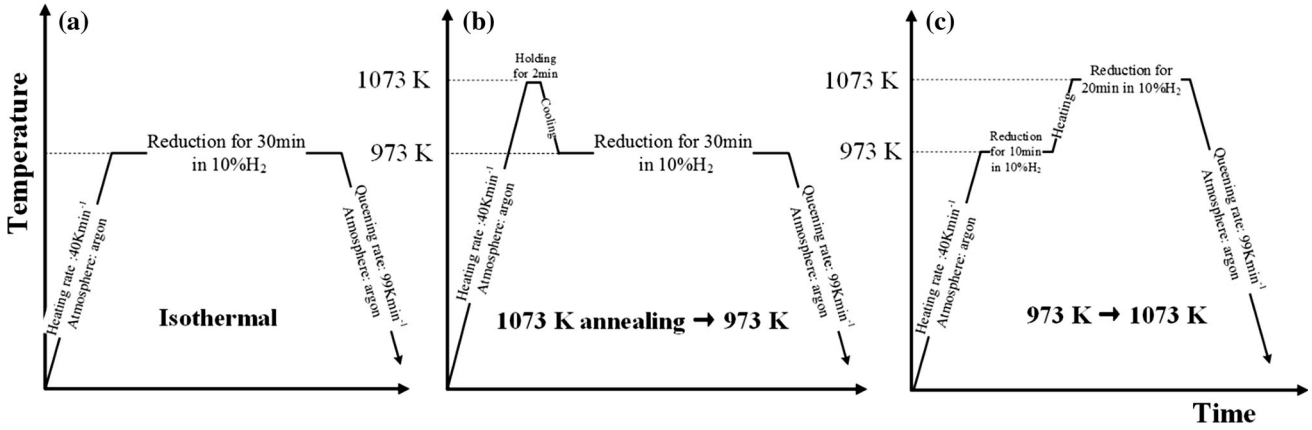

Fig. 1—Schematic illustration of experimental procedure. (*a*) Isothermal reduction of oxide scale; (*b*) the sample was firstly annealed at 1073 K (800 °C) for 2 minutes and then reduced at 973 K (700 °C); (*c*) to confirm the effect of the temperature, the sample was reduced at 973 K (700 °C) first and then elevated to 1073 K (800 °C).

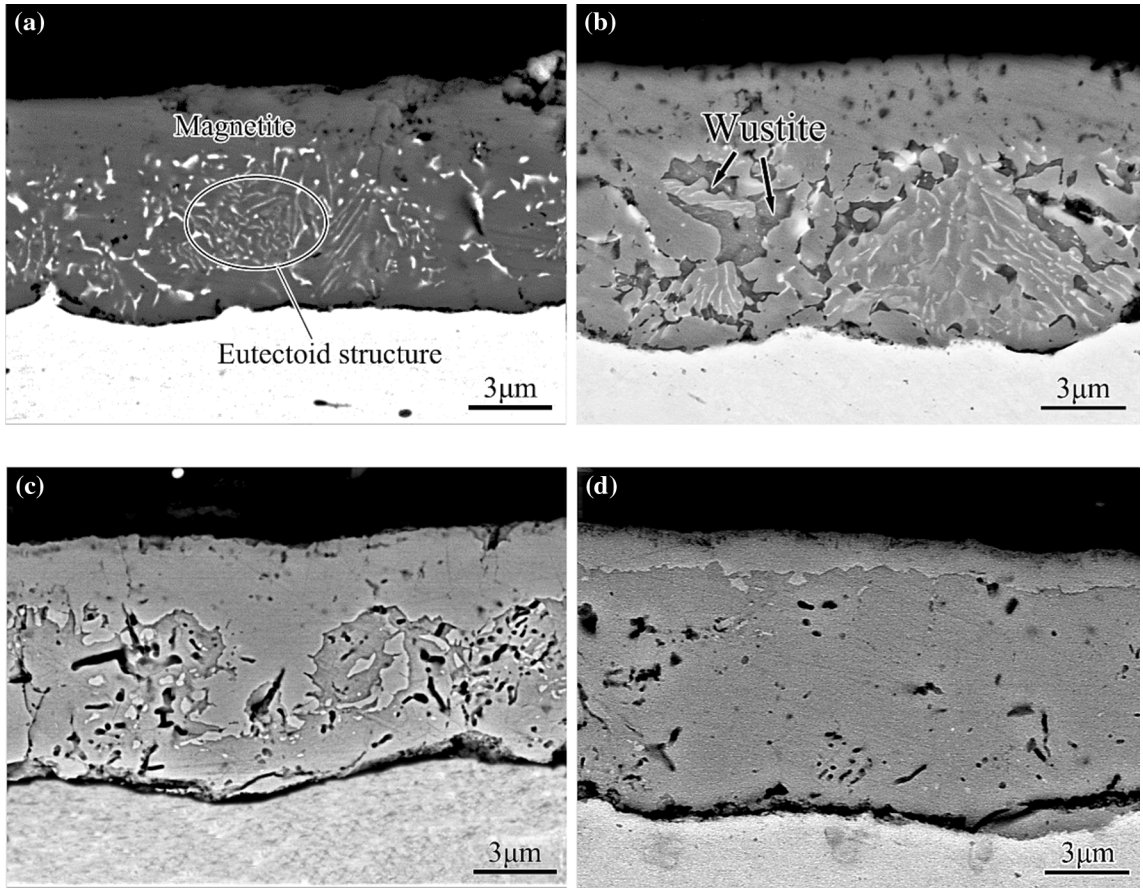

Fig. 2—The cross-sectional, backscattered electron images of the oxide scale: (*a*) as-rolled state; heated and quenched at (*b*) 868 K (595 °C), (*c*) 973 K (700 °C), and (*d*) 1023 K (750 °C).

wüstite. The cavities that appeared in wüstite could either be caused by grinding and polishing during the sample preparation or by the density increase due to transformation.[26] From the Fe-O phase diagram, it is known that wüstite is thermodynamically stable above 843 K (570 °C). During heating, both ''magnetite + iron'' eutectoid and proeutectoid magnetite reversely transformed into wüstite *via* the following reactions[25]:

$$\mathrm{Fe_3O_4} + (1 - 4y)\mathrm{Fe} \rightarrow 4\mathrm{Fe_{1-y}O} \qquad [1]$$

$$(1 - 4y)\mathrm{Fe^{2+}} + 2\mathrm{e^-} + \mathrm{Fe_3O_4} \rightarrow 4\mathrm{Fe_{1-y}O} \qquad [2]$$

Therefore, when reduction is performed below 843 K (570 °C), magnetite primarily participated in the reaction described by the following equation:

$$Fe_3O_4 + H_2 \rightarrow 3Fe + H_2O \quad [3]$$

For the reduction temperature above 843 K (570 °C), wüstite will be directly reduced into iron *via* Eq. [4], while the reduction of magnetite comprises two steps,[5] *i.e.,* Eqs. [5] and [6]):

$$FeO + H_2 \rightarrow Fe + H_2O \quad [4]$$

$$Fe_3O_4 + H_2 \rightarrow 3FeO + H_2O \quad [5]$$

$$FeO + H_2 \rightarrow Fe + H_2O \quad [6]$$

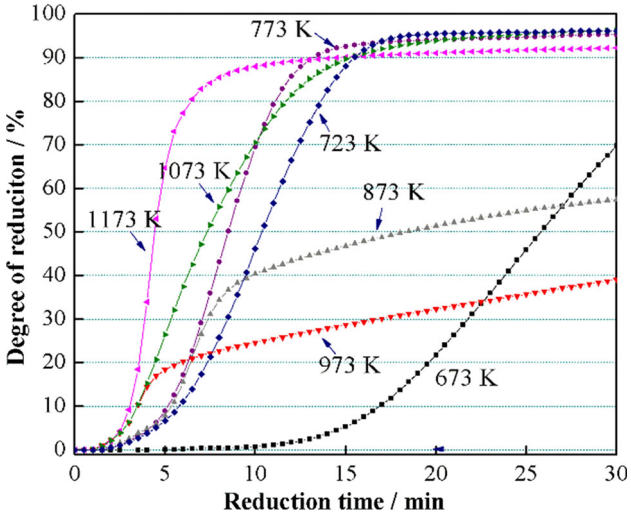

Fig. 3—α–t plots for isothermal reduction of the oxide scale in a gas mixture of 10 pct H_2-Ar.

B. *Reduction of Oxide Scale*

Since a relative high reaction rate is required in industrial application, the reduction of oxide scale by 10 pct hydrogen at above 673 K (400 °C) was investigated in this work. The degree of reduction α was defined by:

$$\alpha = \frac{\Delta W_t}{\Delta W_{\alpha=1}} \quad [7]$$

where ΔW_t is the weight loss at time t; $\Delta W_{\alpha=1}$ is defined as the weight loss when the sample was reduced at 1273 K (1000 °C) until no further weight variation occurs with time.

Figure 3 groups the isothermal α-t plots at different temperatures. The sigmoid kinetic curve can be noticed, which usually includes the induction, acceleration, and decaying stages. The induction stage, which is caused by low hydrogen concentration and the gas hungry, extends with increasing temperature, *e.g.,* nearly 10 minutes at 673 K (400 °C) compared with around 2 minutes at 1173 K (900 °C). Then, the acceleration stage steps in when α reaches approximately 8 pct and lasts until the degree of reduction reaches approximately 90 pct. Nevertheless, as shown in Figure 3, there are two exceptions (*i.e.,* 873 K (600 °C) and 973 K (700 °C)) where the acceleration stage ended exceptionally early. Detailed analysis will be presented in the next section. Finally, at the end of isothermal reduction, the decaying stage shows up and the reduction rate gradually levels out.

As presented in Table I, several mathematical models have been developed for a gas–solid reaction, which is one of the critical steps during the reduction of the oxide scale. By fitting the measured kinetics to these models, one would be able to find out the mechanism of the reduction reaction under the current experimental condition. In general, for a particular controlling mechanism, the corresponding $Y(\alpha)$, which represents the left side of the equations in Table I, can be expected to have a linearity with the reaction time.[26,30,31] The results of applying the mathematical model to the reduction

Table I. Mathematical Modeling of Reaction Kinetics[27–29]

No.	Reduction Mechanism	Equation	Correlation Coefficients 773 K (500 °C)	Correlation Coefficients 1073 K (800 °C)
1	phase-boundary-controlled reaction (infinite slabs)	$\alpha = kt$	0.99715	0.99118
2	phase-boundary-controlled reaction (contracting cylinder)	$1 - (1 - \alpha)^{1/2} = kt$	0.99204	0.99973
3	phase-boundary-controlled reaction (contracting sphere)	$1 - (1 - \alpha)^{1/3} = kt$	0.98628	0.99944
4	one-dimensional diffusion	$\alpha^2 = kt$	0.9628	0.98601
5	two-dimensional diffusion	$\alpha + (1 - \alpha)\ln(1 - \alpha) = kt$	0.92002	0.96827
6	Three-dimensional diffusion	$1 - 3(1 - \alpha)^{2/3} + 2(1 - \alpha) = kt$	0.93468	0.95905
7	random nucleation; unimolecular decay law (first-order)	$[-\ln(1 - \alpha)] = kt$	0.96831	0.99387
8	two-dimensional growth of nuclei (Avrami–Erofeyev equation)	$[-\ln(1 - \alpha)]^{1/2} = kt$	0.99926	0.99332
9	three-dimensional growth of nuclei (Avrami–Erofeyev equation)	$[-\ln(1 - \alpha)]^{1/3} = kt$	0.99872	0.98079

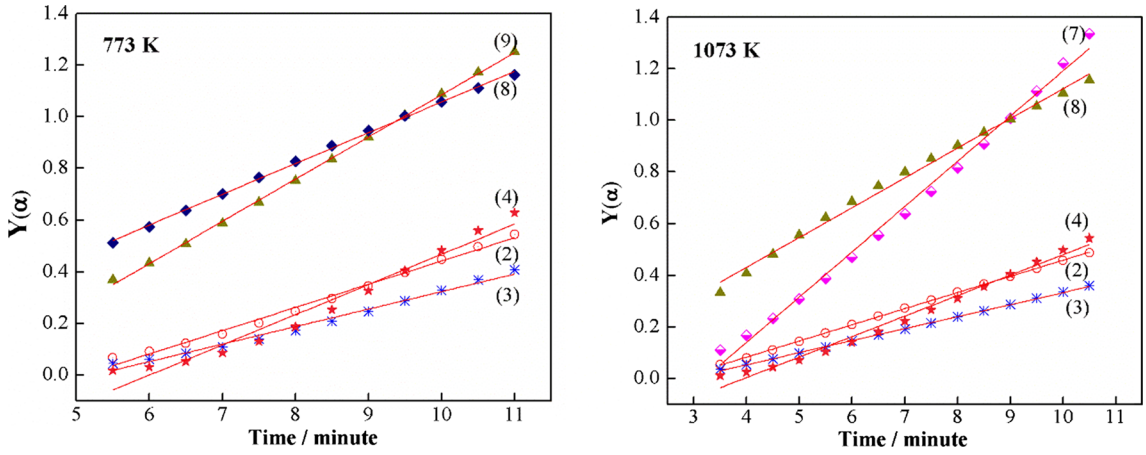

Fig. 4—Mathematical modeling of the reduction kinetics.

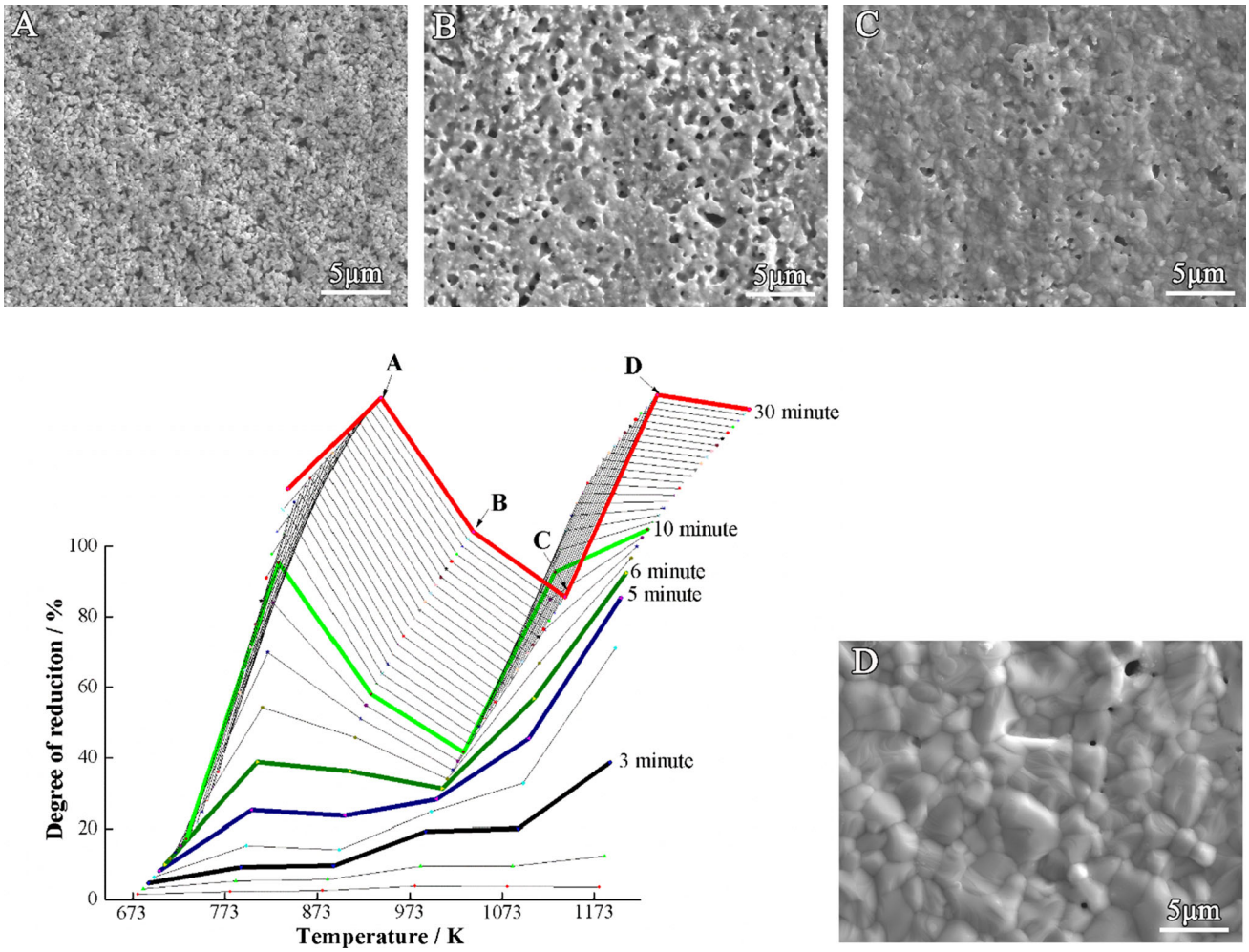

Fig. 5—Degree of reduction *vs* temperature and the surface micrographs of reduction products at (*a*) 773 K (500 °C); (*b*) 873 K (600 °C); (*c*) 973 K (700 °C); (*d*) 1073 K (800 °C).

kinetics at 773 K (500 °C) and 1073 K (800 °C) are presented in Figure 4. The correlation coefficient corresponding to each model is shown in Table I. Model No. 8 achieves the best fit of experimental data obtained at 773 K (500 °C), suggesting a phase-boundary-controlled reaction. For the reduction kinetics at 1073 K (800 °C), model No. 2 representing a three-dimensional growth of nuclei can best describe the experimental data.

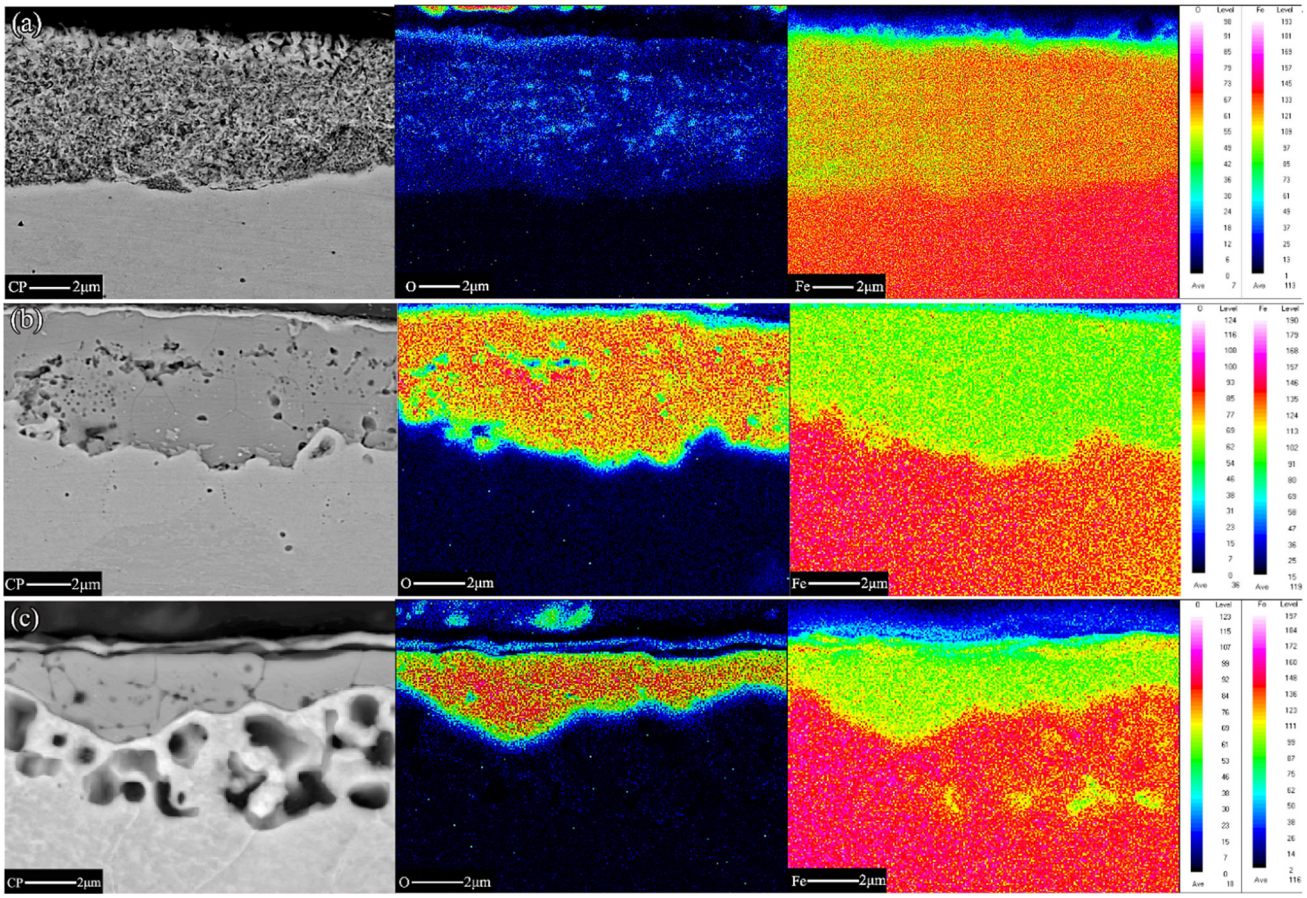

Fig. 6—The cross-sectional backscattered electron images and EPMA mappings of the elements in the reduced scale at (*a*) 773 K (500 °C); (*b*) 973 K (700 °C), and (*c*) 1073 K (800 °C).

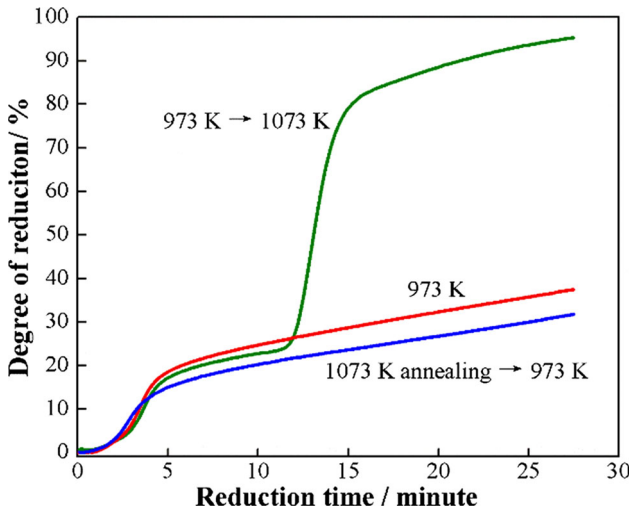

Fig. 7—α–*t* plots obtained from the experiments illustrated in Fig. 1.

C. *Characteristics of the Reduction Products*

Figure 5 presents the degree of reduction as a function of temperature, as well as the corresponding surface morphology of the final reduction product. In the early stages, the reduction progressively increases with increasing temperature. An obvious difference in reduction kinetics appears after 6 minutes of reaction. The reduction process in the temperature range of 873 K (600 °C) to 973 K (700 °C) slows and enters into the decaying period. Similar results were previously reported in the literature,[14,19] where this rate minimum was interpreted to be associated with the dense iron layer, which acts as a barrier against the gas diffusion.

The surface morphology of reduction products changed with the reduction temperature, as shown in Figure 5. The reduction products could be basically classified into two types: porous iron and dense iron, which was obtained below and above 873 K (600 °C), respectively. Under the present experimental conditions, regardless of the transformation during heating, the reactants of the outmost layer are always magnetite, which has a relatively stable stoichiometric composition at low temperatures.[5] Consequently, the difference in morphology should be primarily due to the reaction temperature.

To characterize the reduction product further, samples were analyzed by EPMA, as shown in Figure 6. Figure 6(a) shows the scanning electron micrographs of the cross section of a sample reduced at 773 K (500 °C). The growth of iron into the oxide scale and the randomly distributed iron oxide in the porous iron layer can be clearly seen. The pore size, which is highly

dependent on the reduction condition, *i.e.,* H_2/H_2O ratio, H_2 partial pressure, and temperature, is less than 0.5 μm. At temperatures below 873 K (600 °C), the pore size increases with increasing temperature. This is in good agreement with Guan *et al.*'s result.[23] For the reduction at 973 K (700 °C), only the outmost magnetite layer was reduced into dense iron, whereas the wüstite inside mostly remains unchanged. When the reduction was performed at 1073 K (800 °C), a large portion of the iron oxide was reduced to pure iron, whereas a little wüstite was retained (see Figure 6(c)). Dense iron was also obtained from the outmost magnetite layer. However, the inside wüstite has been reduced into porous iron, which has a large pore size of around 1 μm in diameter. The oxide scale on hot-rolled steel strips usually has defects (*e.g.,* porosity and cracks), such that an easy access of the hydrogen to the advancing interface can be attained. Meanwhile, due to the large quantity of heterogeneous nucleation sites provided by the steel substrate, the iron oxide close to the matrix can easily be reduced.

The morphologies of the product affect the reduction mechanism by influencing the rate-limiting reaction steps. Below the eutectoid temperature *i.e.,* 843 K (570 °C), the magnetite is directly reduced into iron, which exhibits a porous feature. Then, nucleation of iron becomes the rate-limiting step instead of gaseous mass transportation. In the temperature range of 873 K (600 °C) to 973 K (700 °C), the reduction exhibited a relatively high reaction rate at the beginning, but the product is dense iron, once the oxide scale is covered by dense iron, the diffusion of gas reactant is blocked, leading to the slowing of the whole reaction process. At a higher reduction temperature, any thermo-activated diffusion process is promoted and, in addition, the reduction at 1073 K (800 °C) is controlled by phase boundary reactions, which are highly influenced by temperature. As a result, the reaction rate remarkably increased at 1073 K (800 °C).

D. *Effect of Oxide Scale Structure on the Reduction*

As mentioned, the eutectoid structure and proeutectoid magnetite in oxide scale transformed into wüstite during the heating process, and the temperature range where the inverse transformation happens covered the slow reduction valley, as presented in Figure 5. Therefore, it is necessary to find out how the oxide scale structure could affect the reduction kinetics.

Figure 7 shows the α–t plots for the experimental study described earlier. Increasing the temperature should increase the degree of the reduction. By increasing the temperature to 1073 K (800 °C), the reduction degree increased rapidly from 23 to 95 pct. During the annealing process at 1073 K (800 °C), the oxide scale was reduced into a bilayer structure as shown in Figure 2(d). The reduction process, however, exhibits a slow kinetics that is only a little slower than that without 1073 K (800 °C) annealing. However, by increasing the temperature from 973 K (700 °C) to 1073 K (800 °C) after an initial 10 minutes of reduction, the kinetic curve deviated from the original one and a substantial acceleration was achieved. It is generally known that the reduction of magnetite and wüstite follow different kinetics, leading to an unavoidable effect of the oxide scale structure on reduction kinetics. However, this simple experiment suggests that it is not the oxide scale structure but the temperature that plays a more important role in determining the reduction kinetics at higher temperatures (*e.g.,* >973 K (700 °C)).

IV. CONCLUSIONS

As a possible alternative to descaling of the hot-rolled steel strip, the reduction behavior of the oxide scale under a gas mixture of 10 pct H_2-Ar at different temperatures was investigated in this work. The primary conclusions that can be drawn are as follows:

1. During heating under argon, "magnetite + iron" eutectoid and proeutectoid magnetite successively transformed into wüstite. Then, the starting oxide scale structure for isothermal reduction at temperatures above 848 K (575 °C) may include outmost magnetite, eutectoid, and inner wüstite, depending on the extent of the inverse phase transformation during heating.
2. The reduction product varies with temperature and itself affects the kinetics. Porous and dense iron were obtained below and above 873 K (600 °C), respectively. However, at a higher temperature above 973 K (700 °C), it is not the oxide scale structure but the temperature that plays a more important role in determining the reduction kinetics.
3. The kinetic plots of the isothermal reduction of the oxide scale were fitted using mathematical models. Phase-boundary-controlled reaction and three-dimensional growth of nuclei were found to be the controlling mechanism for the reduction at 1073 K (800 °C) and 773 K (500 °C), respectively, while the outer layer dense iron acting as a barrier against the gas diffusion was responsible for the observed "rate-minimum" at 973 K (700 °C).

ACKNOWLEDGMENTS

The authors wish to thank the financial support of the National Science & Technology Pillar program of China (Grant No. 2011BAE13B04) and National Natural Science Foundation of China (Grant No. 51204047 and 51204048) for this work. We also thank Dr. Guan Chuang from Shanghai Jiaotong University for the valuable discussions. In addition, the sponsorship of Baosteel is gratefully acknowledged.

REFERENCES

1. K. Voges, A. Mueth, and B. Lehane: *Iron Steel Technol.*, 2008, vol. 5, pp. 81–96.

2. L.V. Blgdandy and H.J. Engell: *The Reduction of Iron Ores: Scientific Basis and Technology*, Springer-Verlag, Berlin, Heidelberg, 1971, pp. 47–100.
3. M.F. Rau, D. Rieck, and J.W. Evans: *Metall. Mater. Trans. B*, 1987, vol. 18B, pp. 257–78.
4. P.C. Hayes: *Metall. Mater. Trans. B*, 2010, vol. 41B, pp. 19–34.
5. P.C. Hayes: *Steel Res. Int*., 2011, vol. 82, pp. 480–93.
6. Y.K. Rao: *Metall. Mater. Trans. B*, 1979, vol. 10B, pp. 243–55.
7. D.H. St. John and P.C. Hayes: *Metall. Mater. Trans. B*, 1982, vol. 13B, pp. 117–24.
8. S.P. Matthew and P.C. Hayes: *Metall. Mater. Trans. B*, 1990, vol. 21B, pp. 153–72.
9. S.P. Matthew, T.R. Cho, and P.C. Hayes: *Metall. Mater. Trans. B*, 1990, vol. 21B, pp. 733–41.
10. D.H. St. John, S.P. Matthew, and P.C. Hayes: *Metall. Mater. Trans. B*, 1984, vol. 15B, pp. 709–17.
11. R. Nicolle and A. Rist: *Metall. Mater. Trans. B*, 1979, vol. 10B, pp. 429–38.
12. H. Wang and H.Y. Sohn: *ISIJ Int*., 2011, vol. 51, pp. 906–12.
13. M.C. Bagatini, V. Zymla, E. Osorio, and A.C.F. Vilela: *ISIJ Int*., 2011, vol. 51, pp. 1072–9.
14. M. Moukassi, P. Steinmetz, B. Dupre, and C. Gleitzer: *Metall. Mater. Trans. B*, 1983, vol. 14B, pp. 125–32.
15. A. Primavera, S. Cattarino, and M. Pavlicevic: *Ironmaker Steelmaker*, 2007, vol. 34, pp. 290–4.
16. M. Bahgat, Y. Sasaki, S. Hijino, M. Iguchi, and K. Ishii: *ISIJ Int*., 2004, vol. 44, pp. 2023–8.
17. M. Bahgat, Y. Sasaki, S. Hijino, M. Iguchi, and K. Ishii: *ISIJ Int*., 2005, vol. 45, pp. 657–61.
18. Y. Sasaki, M. Bahgat, M. Iguchi, and K. Ishii: *ISIJ Int*., 2005, vol. 45, pp. 1077–83.
19. I. Saeki, T. Ikeda, K. Ohno, T. Sato, and S. Kurosawa: *Tetsu-to-Hagane*, 2011, vol. 97, pp. 12–8.
20. R. Hudson: *Met. Finish*., 1985, vol. 83, pp. 59–61.
21. R. Hudson: *Met. Finish*., 1985, vol. 83, pp. 73–80.
22. J. Shi, D.R. Wang, Y.D. He, H.B. Qi, and G. Wei: *Mater. Lett*., 2008, vol. 62, pp. 3500–2.
23. C. Guan, J. Li, N. Tan, Y.Q. He, and S.G. Zhang: *Int. J. Hydrogen Energy*, 2014, vol. 39, pp. 15116–24.
24. R.Y. Chen and W.Y.D. Yuen: *Oxid. Met*., 2000, vol. 53, pp. 539–60.
25. R.Y. Chen and W.Y.D. Yuen: *Oxid. Met*., 2001, vol. 56, pp. 89–118.
26. W.H. Kim, S. Lee, S.M. Kim, and D.J. Min: *Int. J. Hydrogen Energy*, 2013, vol. 38, pp. 4194–200.
27. J.D. Hancock and J.H. Sharp: *J. Am. Ceram. Soc*., 1972, vol. 55, pp. 74–7.
28. A. Ortega: *Thermochim. Acta*., 1996, vol. 284, pp. 379–87.
29. K. Piotrowski, K. Mondal, H. Lorethova, L. Stonawski, T. Szymanski, and T. Wiltowoski: *Int. J. Hydrogen Energy*, 2005, vol. 30, pp. 1543–54.
30. A. Pineau, N. Kanari, and I. Gaballah: *Thermochim. Acta*., 2006, vol. 447, pp. 89–100.
31. A. Pineau, N. Kanari, and I. Gaballah: *Thermochim. Acta*., 2007, vol. 456, pp. 75–88.